J|A|C|S
ARTICLES
Published on Web 03/26/2004

Electrocatalytic Reductions of Nitrite, Nitric Oxide, and Nitrous Oxide by Thermophilic Cytochrome P450 CYP119 in Film-Modified Electrodes and an Analytical Comparison of Its Catalytic Activities with Myoglobin

Chad E. Immoos,[†] Ju Chou,[‡] Mekki Bayachou,[§] Emek Blair, John Greaves, and Patrick J. Farmer*

Contribution from the Department of Chemistry, University of California, Irvine, California 92697-2025

Received October 7, 2003; E-mail: pfarmer@uci.edu

Abstract: Previous investigations of nitrite and nitric oxide reduction by myoglobin in surfactant film modified electrodes characterized several distinct steps in the denitrification pathway, including isolation of a nitroxyl adduct similar to that proposed in the P450nor catalytic cycle. To investigate the effect of the axial ligand on these biomimetic reductions, we report here a comparison of the electrocatalytic activity of myoglobin (Mb) with a thermophilic cytochrome P450 CYP119. Electrocatalytic nitrite reduction by CYP119 is very similar to that by Mb: two catalytic waves at analogous potentials are observed, the first corresponding to the reduction of nitric oxide, the second to the production of ammonia. CYP119 is a much more selective catalyst, giving almost exclusively ammonia during the initial half-hour of reductive electrolysis of nitrite. More careful investigations of specific steps in the catalytic cycle show comparable rates of nitrite dehydration and almost identical potentials and lifetimes for ferrous nitroxyl intermediate (Fe^{II}-NO^-) in CYP119 and Mb. The catalytic efficiency of nitric oxide reduction is reduced for CYP119 as compared to Mb, attributable to both a lower affinity of the protein for NO and a decreased rate of N−N coupling. Isotopic labeling studies show ammonia incorporation into nitrous oxide produced during nitrite reduction, as has been termed co-denitrification for certain bacterial and fungal nitrite reductases. Mb has a much higher co-denitrification activity than CYP119. Conversely, CYP119 is shown to be slightly more efficient at the two-electron reduction of N_2O to N_2. These results suggest that thiolate ligation does not significantly alter the catalytic reactivity, but the dramatic difference in product distribution may suggest an important role for protein stability in the selectivity of biocatalysts.

Introduction

Heme proteins play many catalytic roles in the biocycling of nitrogen. For instance, assimilatory nitrite reductases (as NiR) catalyze the multielectron reduction of nitrite to ammonia, which is then utilized, or assimilated, by the plants.[1] The dissimilatory nitrite reductases (ds NiR) are part of a multienzyme denitrification pathway that, in combination with nitric oxide reductases (NoR) and nitrous oxide reductases (N_2OR), transforms nitrite to dinitrogen, Scheme 1.[2] Examples of heme-containing enzymes are known for each of these steps; for instance, several assimilatory NiR contain multiple type c hemes,[3] while the dissimilatory NiR contain heme cd_1,[4] a fungal NOR, cytochrome P450nor, contains an Fe-heme coordinated by a cysteinyl thiolate[5] and the N_2OR from *Wolinella* contains an Fe-heme adjacent to a binuclear Cu-heme catalytic center.[6]

Scheme 1

$$NO_2^- \xrightarrow{\text{as NiR}} NH_3$$

$$NO_2^- \xrightarrow{\text{ds NiR}} NO \xrightarrow{\text{NOR}} N_2O \xrightarrow{N_2OR} N_2$$

Cytochrome P450nor, a fungal enzyme which catalyzes the reduction of NO to N_2O, has been the focus of much recent interest, including spectroscopic,[7] mechanistic,[8] and synthetic model studies.[9] The ferric−nitrosyl complex of P450nor reacts

* Corresponding author.
[†] Present address: Department of Chemistry, Duke University, Durham, NC 27710.
[‡] Present address: Department of Chemical Engineering, University of California, Santa Barbara, CA 93106.
[§] Present address: Department of Chemistry, Cleveland State University, Cleveland, OH 44115.

(1) Averill, B. A. *Chem. Rev.* **1996**, *96*, 2951.
(2) (a) Payne, W. J. *Denitrification*; John Wiley & Sons, Inc.: New York, 1981. (b) Zumft, W. G. *Microbiol. Mol. Biol. Rev.* **1997**, *61*, 553.
(3) (a) Einsle, O.; Messerschmidt, A.; Huber, R.; Kroneck, P. M. H.; Neese, F. *J. Am. Chem. Soc.* **2002**, *124*, 11737. (b) Rudolf, M.; Einsle, O.; Neese, F.; Kroneck, P. M. H. *Biochem. Soc. Trans.* **2002**, *30*, 649.
(4) Fülöp, V.; Moir, J. W. B.; Ferguson, S. J.; Hajdu, J. *Cell* **1995**, *81*, 369.
(5) Shoun, H.; Tanimoto, T. *J. Biol. Chem.* **1991**, *266*, 11078.
(6) (a) Liang, J.; Burris, R. H. *J. Bacteriol.* **1989**, *171*, 3176. (b) Drummond, J. T.; Matthews, R. G. *Biochemistry* **1994**, *33*, 3732. (c) Drummond, J. T.; Matthews, R. G. *Biochemistry* **1994**, *33*, 3742.
(7) Obayashi, E.; Tsukamoto, K.; Adachi, S.; Takahashi, S.; Nomura, M.; Iizuka, T.; Shoun, H.; Shiro, Y. *J. Am. Chem. Soc.* **1997**, *119*, 7807.
(8) Daiber, A.; Nauser, T.; Takaya, N.; Kudo, T.; Weber, P.; Hultschig, C.; Shoun, H.; Ullrich, V. *J. Inorg. Biochem.* **2002**, *88*, 343.

10.1021/ja038925c CCC: $27.50

Scheme 2

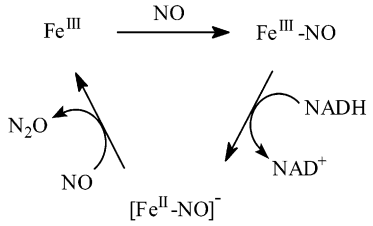

with NADH to generate an identifiable ferrous−nitroxyl intermediate (Fe^{II}-NO^-) which reacts rapidly with nitric oxide to give nitrous oxide, Scheme 2.[8] Although its spectroscopic and structural properties are nearly identical to those of other P450 enzymes, P450nor does not exhibit the usual monooxygenation activity of other P450 enzymes. Theoretical interest has revolved around the effect of the thiolate coordination on the reduced nitroxyl intermediate and its subsequent reactivity.[10]

A number of iron−porphyrin and other transition metal complexes demonstrate nitrite or nitric oxide reductase activity.[11,12] Likewise, simple heme proteins such as myoglobin (Mb) or hemoglobin function such as NO_x reductases when electrochemically reduced in surface-modified electrodes.[13−15] This method has led to key findings on several distinct steps in the denitrification pathway, including isolation of a stable nitroxyl adduct of myoglobin analogous to the intermediate proposed in the P450nor catalytic cycle,[16] a kinetic model of the N−N coupling reaction producing N_2O,[17] and the first example of a heme-catalyzed reduction of nitrous oxide producing dinitrogen and water,[18] which is the ultimate transformation in denitrification.

The proximal histidine ligation of the heme in myoglobin is a poor mimic for the cysteinate coordination found in cytochrome P450nor. To investigate the effect of the axial ligand on the catalysis of nitrite and nitric oxide reductions, we report here the electrochemical NO_x activity of cytochrome P450 CYP119, a thermostable P450 enzyme. CYP119 is isolated from *Sulfolobus solfataricus*, a hyperthermophilic, acidophilic archaebacteria found in sulfurous volcanic hot springs.[19] The crystal structure of CYP119 reveals that the enzyme is smaller and more compact than typical P450 enzymes,[20] which combined with its thermo- and barostability,[21] make CYP119 an excellent candidate for protein film voltammetry.[22]

Experimental Section

Materials. Expressed thermophilic cytochrome P450 CYP119 was obtained from the laboratories of Thomas Poulos at University of California, Irvine, and Paul Ortiz de Montellano at University of California, San Francisco. The expressed enzyme samples were used as received without further purification unless otherwise indicated. Horse skeletal muscle myoglobin was obtained from Sigma. All ^{15}N-labeled compounds were obtained from Isotec. Nitric oxide obtained from Air Gas was further purified by bubbling through a 1 M NaOH solution. [^{15}N}Nitric oxide was generated from L-ascorbic acid and [^{15}N]-sodium nitrite and purified by the same procedure. Angeli's salt, $Na_2N_2O_3$, was prepared and purified by the method of Hunt (recrystallized yield, 89%; $\epsilon = 8550\ M^{-1}\ cm^{-1}$ at 250 nm).[23] Sodium hyponitrite, $Na_2N_2O_2$, was prepared by modification of methods of Scott and Polydoropoulos, (recrystallized yield, 11%; $\epsilon = 6980\ M^{-1}\ cm^{-1}$ at 248 nm).[24] Dimethyldidodecylammonium bromide (DDAB) was purchased from Acros. All other chemicals were reagent grade and used without further purification. Water was purified with a Barnstead Nanopure system to a specific resistance of $>18\ M\Omega/cm^{-2}$.

Electrochemical Apparatus and Procedures. A BAS 100B/W electrochemical system was used for cyclic voltammetry (CV). A three electrode cells consisting of a Pt wire counter electrode, silver/silver chloride reference electrode, and basal plane pyrolytic graphite (PG) electrodes were used for all experiments. The reference compartment was separated from the working compartment by a modified Luggin capillary. Basal plane pyrolytic electrodes were made by sealing a PG cylinder into a glass tube with epoxy and connected to a wire with silver epoxy paste. Electrodes were prepared by roughening the surface with 400-grit SiC paper and cleaning in an ultrasonic bath for 10 min prior to surface modification. Experiments were performed at room temperature in 50 mM sodium phosphate buffer, pH 7.0, containing 100 mM supporting electrolyte, either KCl or NaBr. The solution was purged with nitrogen for at least 20 min to remove oxygen before each experiment. A nitrogen atmosphere was maintained over the solution during all the experiments. Digital simulations of voltammograms at pH 7 were performed using the BAS Digisim program; each simulation was repeated until the simulated peak current and peak potential matched that of experimental results.

Protein/DDAB Film Preparation. A 10 μL portion of 0.01 M DDAB solution and another 10 μL portion of 8 mg/mL protein solution were cast onto the surface of a basal plane pyrolytic graphite (PG) electrode. The wet film electrode was covered with a test tube and allowed to stand overnight before being uncovered and allowed to dry in air. Film electrodes were allowed to dry for at least 24 h prior to use. Protein film electrodes of the NO adducts of enzymes were also prepared in an anaerobic glovebox under nitrogen for single-turnover experiments. Ferrous nitrosyl adducts were prepared by the addition of sodium dithionite and sodium nitrite to a solution of the enzyme followed by purification by size-exclusion chromatography.

Rotating Disk Electrode Voltammetry. Rotating disk electrode experiments utilized a basal plane pyrolytic graphite disk as the working

(9) Suzuki, N.; Higuchi, T.; Urano, Y.; Kikuchi, K.; Uchida, T.; Mukai, M.; Kitagawa, T.; Nagano, T. *J. Am. Chem. Soc.* **2000**, *122*, 12059.
(10) (a) Harris, D. L. *Int. J. Quantum Chem.* **2002**, *88*, 183. (b) Silaghi-Dumitrescu, R. *Eur. J. Inorg. Chem.* **2003**, 1048.
(11) (a) Murphy, W. R., Jr.; Takeuchi, K.; Barley, M. H.; Meyer, T. J. *J. Am. Chem. Soc.* **1982**, *104*, 5817. (b) Barley, M. H.; Takeuchi, K.; Meyer, T. J. *J. Am. Chem. Soc.* **1986**, *108*, 5876. (c) Barley, M. H.; Rhodes, M. R.; Meyer, T. J. *Inorg. Chem.* **1987**, *26*, 1746. (d) Younathan, J. N.; Wood, K. S.; Meyer, T. J. *Inorg. Chem.* **1992**, *31*, 3280. (e) Bedioui, F.; Trevin, S.; Albin, V.; Villegas, M. G. G.; Devynck, J. *Anal. Chim. Acta* **1997**, *341*, 177.
(12) (a) Toth, J. E.; Anson, F. C. *J. Am. Chem. Soc.* **1989**, *111*, 2444. (b) Rhodes, M. R.; Barley, M. H.; Meyer, T. J. *Inorg. Chem.* **1991**, *30*, 629. (c) Sunohara, S.; Nishimura, K.; Yahikozawa, K.; Ueno, M.; Eny, M.; Takasu, Y. *J. Electroanal. Chem.* **1993**, *354*, 161. (d) Keita, B.; Belhouri, A.; Nadjo, L.; Constant, R. *J. Electroanal. Chem.* **1995**, *381*, 243.
(13) (a) Lin, R.; Bayachou, M.; Greaves, J.; Farmer, P. J. *J. Am. Chem. Soc.* **1997**, *119*, 12689. (b) Farmer, P. J.; Lin, R.; Bayachou, M. *Comments Inorg. Chem.* **1998**, *20*, 101.
(14) Mimica, D.; Zagal, J. H.; Bedioui, F. *J. Electroanal. Chem.* **2001**, *497*, 106.
(15) (a) Zhou, Y. L.; Hu, N. F.; Zeng, Y. H.; Rusling, J. F. *Langmuir* **2002**, *18*, 211. (b) Huang, R.; Hu, N. F. *Biophys. Chem.* **2003**, *104*, 199. (c) Huang, R.; Hu, N. F. *Bioelectrochemistry* **2001**, *54*, 75. (d) Liu, H. Y.; Wang, L. W.; Hu, N. F. *Electrochim. Acta* **2002**, *47*, 2515.
(16) Lin, R.; Farmer, P. J. *J. Am. Chem. Soc.* **2000**, *122*, 2393.
(17) Bayachou, M.; Lin, R.; Cho, W.; Farmer, P. J. *J. Am. Chem. Soc.* **1998**, *120*, 9888.
(18) Bayachou, M.; Elkbir, L.; Farmer, P. J. *Inorg. Chem.* **2000**, *39*, 289.
(19) (a) Wright, R. L.; Harris, K.; Solow, B.; White, R. H.; Kennelly, P. J. *FEBS Lett.* **1996**, *384*, 235. (b) McLean, M. A.; Mavew, S. A.; Weiss, M. K.; Krepich, S.; Sligar, S. G. *Biochem. Biophys. Res. Commun.* **1998**, *252*, 166.
(20) (a) Yano, J. K.; Koo, L. S.; Schuller, D. J.; Li, H.; Ortiz de Montellano, P. R.; Poulos, T. L. *J. Biol. Chem.* **2000**, *275*, 31086. (b) Park, S.; Yamane, K.; Adachi, S.; Shiro, Y.; Weiss, K. E.; Sligar, S. G. *Acta Crystallogr.* **2000**, *D56*, 1173.
(21) Koo, L. S.; Tschirret-Guth, R. A.; Straub, W. E.; Moenne-Loccoz, P.; Loehr, T. M.; Ortiz de Montellano, P. R. *J. Biol. Chem.* **2000**, *275*, 14112.
(22) Koo, L. S.; Immoos, C. E.; Cohen, M. S.; Farmer, P. J.; Ortiz de Montellano, P. R. *J. Am. Chem. Soc.* **2002**, *124*, 5684.
(23) Hunt, H. R., Jr.; Cox, J. R., Jr.; Ray, J. D. *Inorg. Chem.* **1962**, *1*, 938.
(24) (a) Scott, A. W. *J. Am. Chem. Soc.* **1927**, *49*, 986. (b) Polydoropoulos, C. N. *Chem. Chron.* **1959**, *24*, 147.

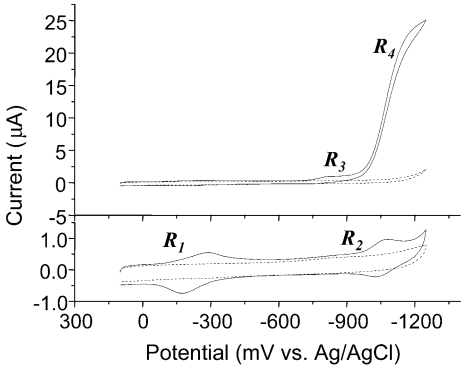

Figure 1. Cyclic voltammograms of CYP119/DDAB in the absence (dotted) and presence (solid) of 34 mM sodium nitrite. Conditions: 50 mM phosphate; pH 7.0; 100 mM NaBr; scan rate = 50 mV/s. Control experiments are shown as a dashed line, under the same conditions on a DDAB-modified electrode without CYP119.

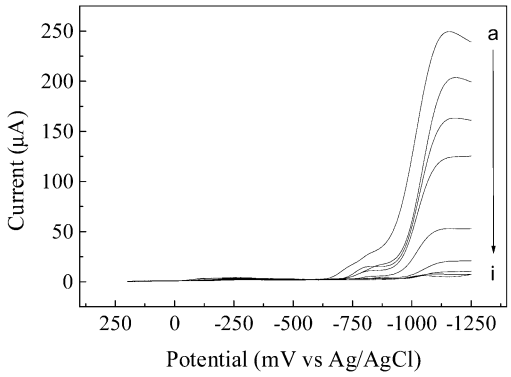

Figure 2. Cyclic voltammograms of the pH dependence of CYP119/DDAB in the presence of 34 mM sodium nitrite at (a) pH 5.2, (b) pH 6.0, (c) pH 6.5, (d) pH 7.0, (e) pH 7.5, (f) pH 8.2, (g) pH 8.9, (h) pH 9.6, and (i) no nitrite. Conditions: 50 mM buffer; 100 mM NaBr; scan rate = 100 mV/s.

electrode. The working electrode was prepared in a manner similar to that mentioned previously for the preparation of protein film electrodes. Experiments were carried out with a conventional three-electrode configuration as described above. Rotating disk electrode experiments were conducted using a Radiometer rotating disk electrode. Only rotation rates up to 400 rpm were used to prevent the protein film from separating from the electrode surface at higher rotation speeds.

Bulk Electrolysis. For bulk electrolysis reactions, pyrolitic graphite plates (1.0 cm × 1.0 cm × 0.2 cm) coated with Mb or CYP119 and DDAB were used as working electrodes.[17] Controlled potential was applied by using a BAS 100 W and a Power Module potentiostat, an Ag/AgCl reference, and a Pt grid counter electrode separated by a fine frit from the main compartment. The headgas over the electrolysis solution was sampled in a loop and transferred directly into a Micromass Autospec mass spectrometer via a GC interface through a Plot GC column (fused silica 50 m × 0.32 mm—Al_2O_3, KCl coating). Data were acquired in EI mode at 1000 resolution. ^{15}NO was generated by treatment of $Na^{15}NO_2$ with $Fe(SO_4)/H_2SO_4$, with a He carrier gas used to transfer the ^{15}NO into the electrolysis cell through a fused silica line.[17]

Nitrite Reduction. For the concentration dependence of nitrite reduction, aliquots of concentrated nitrite solution (1 M) were added via a gastight syringe. At each concentration, the solution was stirred vigorously upon addition and degassed for at least 5 min before each experiment. Colorimetric determinations of solution-based nitrite, hydroxylamine, and ammonia were conducted as previously described.[13]

Nitric Oxide and Nitrous Oxide Reduction. An excess of pre-purified nitric oxide or nitrous oxide was bubbled through a thoroughly degassed solution of 50 mM phosphate, pH 7, with 100 mM NaBr as supporting electrolyte within the electrochemical cell. Special care was taken to ensure that the electrochemical cell was airtight and free from oxygen before the addition of nitric oxide. After addition, the solution was kept under static nitrogen pressure throughout the experiments.

Results

Deposition of CYP119/DDAB films was analogous to those of Mb/DDAB;[13,16] films deposited on quartz displayed a ferric P450 Soret band at 418 nm, with distinctive Q-band splitting between 500 and 600 nm, both of which suggest retention of the native thiolate-ligated heme environment (Supplemental S1). A typical cyclic voltammogram for a CYP119/DDAB film on a basal plane pyrolytic graphite electrode in pH 7 buffered solution (100 mM NaBr electrolyte) is shown in Figure 1. Two well-defined reduction couples are evident, assigned to the Fe^{III}/Fe^{II} redox couple, $\mathbf{R_1}$, at −0.21 V vs Ag/AgCl, and the Fe^{II}/Fe^{I} redox couple, $\mathbf{R_2}$ at −1.04 V vs Ag/AgCl. The $\mathbf{R_1}$ couple displays current controlled by linear diffusion at scan rates above 500 mV/s, where the current is proportional to the square root of the scan rate (Supporting Information S2). At rates below 500 mV/s, the current is proportional to the scan rate, typical of the thin-film behavior seen for other DDAB/protein systems.[17] As seen previously for Mb/DDAB films, the $\mathbf{R_1}$ couple varies linearly ca. −48 mV/pH unit in the range from pH 5.5 to 10, but the $\mathbf{R_2}$ couple remains constant over this range (Supporting Information S3).

Nitrite Reduction. Addition of sodium nitrite to the electrochemical cell changes the electrochemical response of CYP119/DDAB, Figure 1. The current at the Fe^{III}/Fe^{II} couple decreases upon addition of nitrite but does not shift in potential. At more negative potentials two new catalytic waves are seen which are dependent on nitrite concentration, with the half-wave potential of $\mathbf{R_3}$ at ca. −0.86 V and that for $\mathbf{R_4}$ at ca. −1.11 V. The electrocatalytic current at $\mathbf{R_4}$ exhibits saturation kinetics, increasing to a limiting value at ∼34 mM. The $k_{cat.}$ for nitrite reduction by CYP119 can be calculated from a Lineweaver−Burke plot, yielding a K_m value of 11.5 mM (Supporting Information S4 and S5).

The electrocatalytic currents are strongly pH dependent, as shown in Figure 2. At pH 5.2, the maximum peak current ratios compared to the noncatalytic current for the Fe^{II}/Fe^{I} peak are ∼4 for $\mathbf{R_3}$ and ∼40 for $\mathbf{R_4}$. The catalytic efficiency for $\mathbf{R_3}$ is more strongly affected by pH, decreasing significantly as the pH is increased, as expected for a proton-dependent process. At pH > 9, the current does not exceed that of the Fe^{II}/Fe^{I} reduction process in the absence of nitrite. The solution pH affects the two catalytic reduction peaks differently. The potential of $\mathbf{R_4}$ shifts ∼−40 mV/pH unit with a small decrease in catalytic current with increasing pH. The potential of $\mathbf{R_3}$ has smaller pH dependence, shifting ∼−20 mV/pH unit with the catalytic current decreasing significantly with increasing pH. Voltammograms of CYP119/DDAB are unaffected by the presence of ammonia at 50 mM (Supporting Information S6); hydroxylamine at 34 mM does induce a small catalytic response beginning at the $\mathbf{R_1}$ potential (Supporting Information S7). Under the conditions used during analytical voltammetric experiments, neither of these products is expected to influence the current response observed.

In nitrite solutions, limiting the potential window from +0.20 to −0.60 V results in loss of the Fe^{III}/Fe^{II} redox couple after successive scans, Figure 3. Holding the electrode potential at

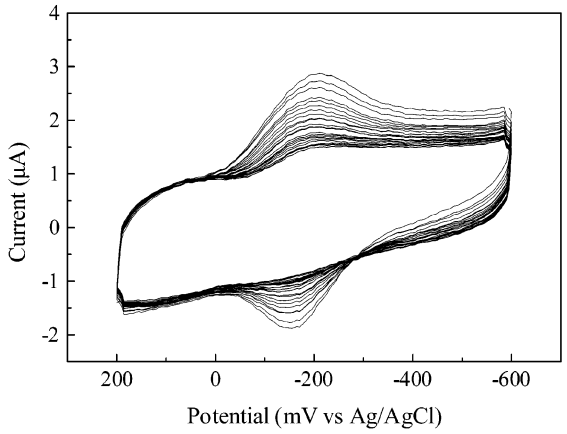

Figure 3. Successive scans of CYP119/DDAB in the presence of 34 mM nitrite, showing loss of the $Fe^{3+/2+}$ couple. Conditions: 50 mM phosphate; pH 7.0; 100 mM NaBr; scan rate = 100 mV/s.

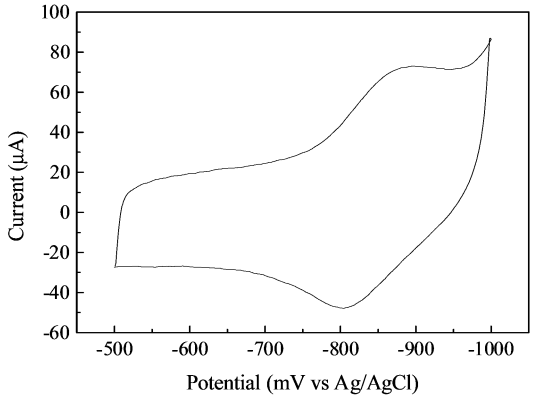

Figure 4. Rapid scan of CYP119/DDAB in the presence of 34 mM nitrite after holding the potential at −0.4 V for 20 s. Conditions: 50 mM sodium phosphate; pH 7.0; 100 mM NaBr; scan rate = 5 V/s.

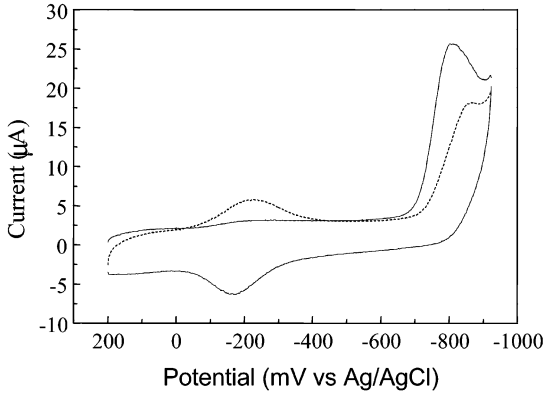

Figure 5. Regeneration of the Fe^{3+}/Fe^{2+} redox couple after holding the potential at −0.4 V for 60 s. First two scan segments are in solid lines; the third scan segment is dashed. Conditions: 50 mM sodium phosphate; pH 7.0; 100 mM NaBr; scan rate = 100 mV/s.

−0.40 V for 20 s prior to scanning results in a reversible redox couple at −0.85 V, Figure 4. Equivalent cathodic and anodic currents for this couple, with $i_{pa}/i_{pc} \sim 1$, is only observed at scan rates >1 V/s; at slower scan rates, the reduction is irreversible and the Fe^{III}/Fe^{II} redox couple reappears, Figure 5.

Rotating disk voltammetry of Mb/DDAB were performed in the presence of varying concentrations of nitrite, Figure 6. The steady-state catalytic wave at −1.1 V vs Ag/AgCl shows an increase of the limiting current with increasing nitrite concentrations; in agreement with previous reports. In contrast, the cathodic current associated with the Fe^{III}/Fe^{II} redox couple decreases with increasing nitrite concentration.

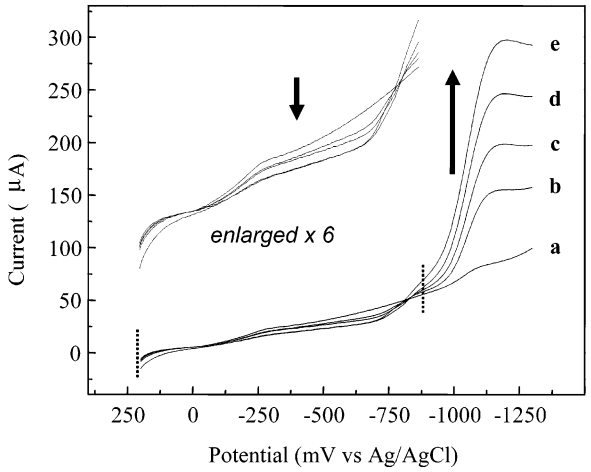

Figure 6. Rotating disk electrode voltammetry of Mb/DDAB under varying concentrations of nitrite: (a) none; (b) 2 mM; (c) 4 mM; (d) 8 mM; (e) 12 mM. Conditions: 50 mM phosphate buffer; pH 7; 100 mM NaBr; scan rate = 20 mV/s; rotation rate, 400 rpm. Enlarged plot shows the loss of current at −250 mV with increasing nitrite concentration.

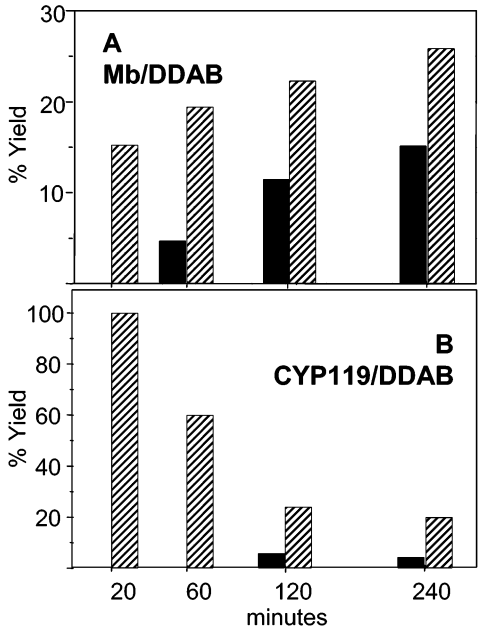

Figure 7. Analysis of ammonia (striped) and hydroxylamine (solid) at different time points during bulk electrolysis of a 10 mM $NaNO_2$ solution, pH 6.0 (100 mM phosphate buffer) using (A) Mb/DDAB and (B) CYP119/DDAB electrodes at −1.2V vs Ag/AgCl. Yields given as percentage of nitrite consumed at equivalent times; data in B average of four trials. Note the difference in *y*-axis scales.

Product Analysis. Controlled-potential electrolysis experiments at the potential of −1.2 V of CYP119/DDAB in nitrite solutions at pH 6 were used to determine the products of the catalysis. The aqueous products ammonia and hydroxylamine were determined by the standard colorimetric methods. A comparison of the product distributions under identical experiments using CYP119 and Mb as electrocatalyst is shown in Figure 7.

To identify the gaseous products of the catalytic reduction of nitrite, ^{15}N-labeled sodium nitrite solution at pH 6 was electrolyzed at −1.2 V; separate experiments were performed

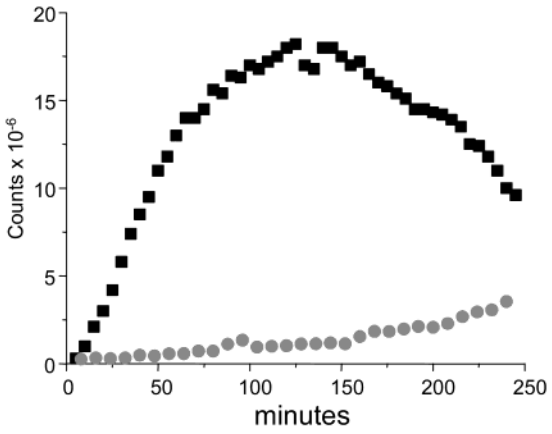

Figure 8. Relative yields of $^{15}N_2O$ from GC/MS analysis of sampled headgas over bulk electrolysis at −1.2 V of a 10 mM $Na^{15}NO_2$, pH 6.0 using Mb/DDAB (squares) or CYP119/DDAB (circles) electrocatalysts of comparable loadings.

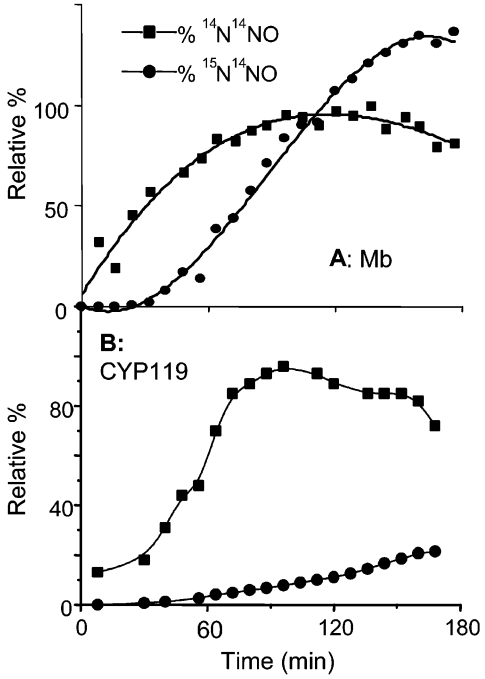

Figure 9. Time-based analysis of relative yields of $^{14}N^{14}NO$ and $^{15}N^{14}NO$ from GC/MS analysis of sampled headgas over 3 h of bulk electrolysis at −1.2 V of a 10 mM $Na^{14}NO_2$ with 10 mM $^{15}NH_4Cl$ solution, pH 6.0: (A) using the Mb/DDAB electrode; (B) using the CYP119/DDAB electrode. The *y*-axis is the relative yield as a percentage of the maximum $^{14}N^{14}NO$ counts in MS.

using CYP119/DDAB and Mb/DDAB as catalysts using similar catalyst loadings. The time-based formation of $^{15}N_2O$ from both experiments is shown in Figure 8. The headgas over the reaction vessel was sampled into a loop and then transferred into the mass spectrometer via the GC interface using a fused silica column; a 106 ppm concentration of Ar in the He mixture carrier gas was used as a mass standard (Supporting Information S8). After a few minutes of electrolysis, signals at $m/z = 46$, corresponding to $^{15}N_2O$, were seen and grew with time (Supporting Information S9) along with small peaks corresponding to the fragments $[^{15}NO]^+$ and $[^{15}N_2]^+$. Column-separated peaks of $[^{15}NO]^+$ (m/z 31) and $[^{15}N_2]^+$ (m/z 30) are also readily identified, indicating that both compounds are produced in-

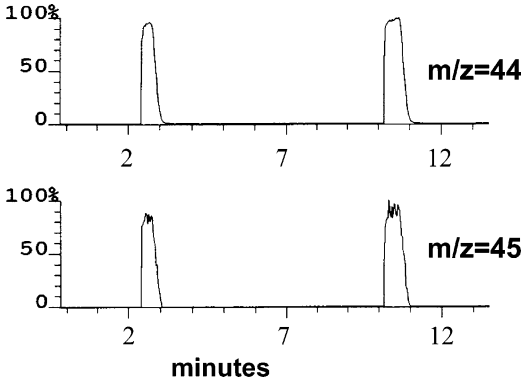

Figure 10. Gas chromatograms of sampled headgas above the reaction of natural abundance $Na_2N_2O_2$ with $^{15}NH_4Cl$ in pH 10 buffered solution, demonstrating the formation of both $^{14}N_2O$, $m/z = 44$, and mixed-label $^{14,15}N_2O$, $m/z = 45$. Minutes mark time from the mixing of reagents before sampling of the headgas.

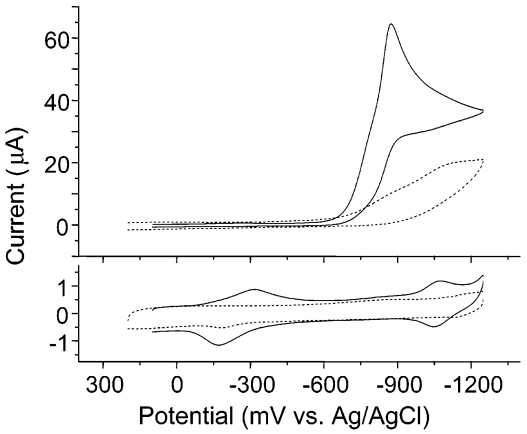

Figure 11. Cyclic voltammograms of CYP119/DDAB in the absence (bottom, solid line) and presence of a saturated solution nitric oxide (top, solid line). Conditions: 50 mM sodium phosphate; pH 7.0; 100 mM NaBr; scan rate = 100 mV/s. Control experiments are shown as a dashed line, under the same conditions without CYP119.

dependently during the bulk electrolysis, demonstrated for Mb/DDAB in Supporting Information S10.

Ammonia Incorporation. To probe incorporation of ammonium into formation of N_2O, a mixed solution of ^{15}N-labeled NH_4Cl and ^{14}N-labeled NO_2^- was subjected to bulk electrolysis by CYP119/DDAB and Mb/DDAB. Analysis of the headgas by GC-MS shows growing signals identified as both $^{14}N^{14}NO$ and $^{15}N^{14}NO$, in which one N from ^{15}N-labeled NH_4Cl is incorporated, Figure 9.

To test for possible chemical species responsible for the incorporation, experiments utilizing the two possible intermediates, hyponitrite and trioxodinitrate, were undertaken. Each was then dissolved in pH 13 buffer in an airtight reaction cell and $^{15}NH_4^+$ or $^{15}NH_3OH^+$ added during their decomposition to probe the incorporation of ^{15}N into the gas product N_2O. The reaction cell was connected to a mass spectrometer with fused silica line through a GC interface. Addition of $^{15}NH_3OH^+$ to both solutions generated mixed label $^{14,15}N_2O$, but only hyponitrite generated the mixed label gaseous product upon addition of $^{15}NH_4^+$, Figure 10 and Supporting Information S11 and S12.

NO Reduction. Addition of NO(g) to a thoroughly degassed solution of 50 mM sodium phosphate buffer, pH 7, changes the voltammetric response as seen in Figure 11. An irreversible catalytic wave at −0.81 V, close to the $\mathbf{R_3}$ couple seen in the

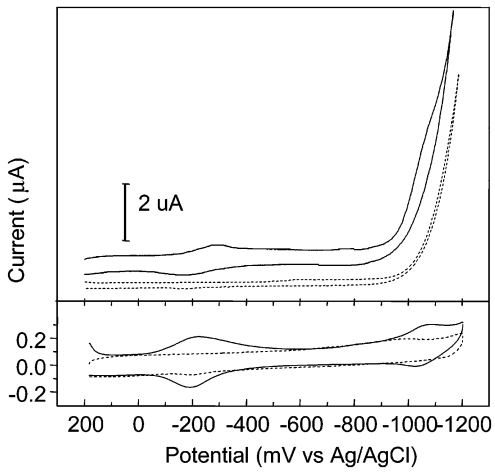

Figure 12. Cyclic voltammograms of CYP119/DDAB in the absence (dotted) and presence (solid) of a saturated solution of N_2O. Conditions: 50 mM sodium phosphate; pH 7.0; 100 mM NaBr; scan rate = 20 mV/s.

electrocatalytic reduction of nitrite by CYP119/DDAB, that demonstrates the catalytic reduction of nitric oxide. The catalysis exhibits a strong dependence on scan rate. An increase in the scan rate results in attenuation of the catalytic peak and the reappearance of the Fe^{III}/Fe^{II} redox couple. Attempts to observe a reversible redox couple for the nitrosyl to nitroxyl transformation in the presence of excess nitric oxide were unsuccessful, even at scan rates as high as 20 V/s. In experiments using ^{15}NO generated in a separate vessel from ^{15}N-labled sodium nitrite, mass spectral analysis of the headgas showed a large buildup of $^{15}N_2O$ (data not shown).

N_2O Reduction. The CVs of CYP119/DDAB electrode in the absence and presence of N_2O are shown in Figure 12. The addition of N_2O causes no change in the Fe^{III}/Fe^{II} current but a significant increase in current along with a loss of reversibility of Fe^{II}/Fe^{I}. The large current is assigned as the catalytic reduction of N_2O.

Discussion

Electrochemical and Catalytic Activity of CYP119/DDAB. Surfactant films have proven useful in obtaining direct electrochemistry from a number of heme proteins, including myoglobin,[25] hemoglobin,[26] and peroxidases.[27] Rusling first reported the electrochemistry of P450cam on film-modified electrodes[28] and we have previously obtained similar results for P450 CYP119 in DDAB films.[22] A typical cyclic voltammogram for CYP119/DDAB film on a basal plane pyrolytic graphite electrode in pH 7 buffered solution (100 mM NaBr electrolyte) is shown in Figure 1A. In analogy to previous reports on myoglobin and P450cam film electrodes, we assign the reduction couples to the Fe^{III}/Fe^{II} and Fe^{II}/Fe^{I} redox couples, eqs 1 and 2.

$$Fe^{III} + e^- \rightleftharpoons Fe^{II} \quad (1)$$

$$Fe^{II} + e^- \rightleftharpoons Fe^{I} \quad (2)$$

$$NO_2^- + ne^- + mH^+ \rightarrow NH^{4+} + NH_3OH^+ + N_2O + NO + N_2 \quad (3)$$

Like Mb, CYP119 in DDAB films acts as a highly active catalyst for the reduction of nitrite in aqueous solutions, and a similar range of products are produced, eq 3. By analogy, we can identify two catalytic waves, the first, $\mathbf{R_3}$ corresponds to the reduction of the nitric oxide adduct and the second $\mathbf{R_4}$ to the production of ammonia. The catalytic efficiency of CYP119, measured at 20 mV/s scan rate as current per mole substrate per second, is 140 as opposed to over 500 for Mb. Thus thiolate ligation does not enhance or significantly alter the catalytic behavior.

But, time-based analysis of the products of CYP119 electrocatalysis yielded unexpected results, Figure 7. First, ammonia is the initial product formed with high apparent yield; hydroxylamine is not detectable in the first hour, and only a small yield of hydroxylamine is obtained after 2 h. In the first 20 min, almost all the consumed nitrite is being used to produce ammonia, but the percent of ammonia from consumed nitrite decreased dramatically as the reaction progressed. For example, 99% of consumed nitrite is being used to produce ammonia after 20 min, but only about 20% after 4 h. In comparison, using Mb/DDAB as a catalyst generates considerable gaseous products immediately; after 20 min the aqueous products (ammonia and hydroxylamine) account for less than 20% of the nitrite consumed.[13]

Time-based analysis of the gaseous products are also instructive; for Mb/DDAB formation of the main product, N_2O, begins with the initial electrolysis, but for CYP119/DDAB gas production begins slowly and never reaches comparable levels, Figure 8. Thus, despite the similarity in electrochemical response, there is a large difference in product distribution between the two heme protein catalysts. To more fully understand this reactivity, several specific steps in the complex reduction of nitrite were probed by electrochemical methods, as described below.

Binding and Dehydration of Nitrite. The apparent similarity of Mb and CYP119 in the electrocatalytic reduction of nitrite is not found in solution binding studies of their ferric states. For met Mb, the presence of 30 mM nitrite shifts the Soret peak absorbance to 412 nm, and the Fe^{III}/Fe^{II} couple of Mb/DDAB by ca. −50 mV, both consistent with the binding of nitrite to the ferric heme, eq 4. The catalytic current dependence on nitrite concentration yields an apparent $K_m = 3.3$ mM, very close to the known K_d of nitrite to met Mb in solution.[13] For CYP119, a similar analysis yields an apparent $K_m = 11.5$ mM, but there are no corresponding shifts in Soret absorbance or Fe^{III}/Fe^{II} couple up to 40 mM nitrite (Supporting Information S13). Although there are previous reports of spectral changes for P450cam in the presence of nitrite,[29] these are irreproducible for CYP119. Thus the initial step in the catalysis is likely not reduction of the ferric−nitrite adduct, as in eq 5. Instead, the

(25) (a) Rusling, J. F.; Nassar, A. E. F. *J. Am. Chem. Soc.* **1993**, *115*, 11891. (b) Nassar, A. E. F.; Bobbit, J. M.; Stuart, J. D.; Rusling, J. F. *J. Am. Chem. Soc.* **1995**, *117*, 10986. (c) Nassar, A. E. F.; Zhang, Z.; Chynwat, V.; Frank, H. A.; Rusling, J. F.; Suga, K. *J. Phys. Chem.* **1995**, *99*, 11013. (d) Nassar, A. E. F.; Narikiyo, Y.; Sagara, T.; Nakashima, N.; Rusling, J. F. *J. Chem Soc., Faraday Trans.* **1995**, *91*, 1775. (e) Nassar, A. E. F.; Willis, W. S.; Rusling, J. F. *Anal. Chem.* **1995**, *67*, 2386.

(26) Lu, Z. Q.; Huang, Q. D.; Rusling, J. F. *J. Electroanal. Chem.* **1997**, *423*, 59.

(27) (a) Zhang, Z.; Chouchane, S.; Magliozzo, R. S.; Rusling, J. F. *Chem. Commun.* **2001**, 177. (b) Zhou, Y. L.; Hu, N. F.; Zeng, Y. H.; Rusling, J. F. *Langmuir* **2002**, *18*, 211.

(28) (a) Zu, X. L.; Lu, Z. Q.; Zhang, Z.; Schenkman, J. B.; Rusling, J. F. *Langmuir* **1999**, *15*, 7372. (b) Lvov, Y. M.; Lu, Z. Q.; Schenkman, J. B.; Zu, X. L.; Rusling, J. F. *J. Am. Chem. Soc.* **1998**, *120*, 4073. (c) Zhang, Z.; Nassar, A. E. F.; Lu, Z. Q.; Schenkman, J. B.; Rusling, J. F. *J. Chem. Soc., Faraday Trans.* **1997**, *93*, 1769.

(29) Sono, M.; Dawson, J. H. *J. Biol. Chem.* **1982**, *257*, 5496.

lack of a shift in the Fe^{III}/Fe^{II} redox couple in the presence of nitrite, in addition to the lack of a change in the UV−visible spectra, suggests a simple reduction of Fe^{III} to Fe^{II} followed by a bimolecular reductive dehydration of nitrite yielding a ferric−NO complex, as was previously suggested for nitrite catalysis by water-soluble iron−porphyrins, eq 6.[11b]

$$Fe^{III} + NO_2^- \rightarrow Fe^{III}\text{-}NO_2^- \quad (4)$$

$$Fe^{III}\text{-}NO_2^- + e^- \rightarrow Fe^{II}\text{-}NO_2^- \quad (5)$$

$$Fe^{II} + NO_2^- + H^+ \rightarrow Fe^{III}\text{-}NO + OH^- \quad (6)$$

$$Fe^{III}\text{-}NO + e^- \rightarrow Fe^{II}\text{-}NO \quad (7)$$

Using rotating disk electrochemistry, Bedioui and co-workers reported that Mb/DDAB in the presence of nitrite does show a current enhancement at Fe^{III}/Fe^{II} potentials.[14] These reductive waves, assigned to the single electron reduction of the $[Fe^{III}\text{-}(NO)]^+$ adduct, had very slow charge-transfer characteristics and were not observable by cyclic voltammetry. Our attempts to repeat these experiments have given significantly different results, Figure 6. The steady-state wave at −1.1 V vs Ag/AgCl shows an increase of the limiting current with increasing nitrite concentrations, in agreement with a previous report. In contrast, the cathodic current associated with the Fe^{III}/Fe^{II} redox couple decreases with increasing nitrite concentration. We attribute loss of the Fe^{III}/Fe^{II} cathodic wave during rotating disk voltammetry experiments to a buildup of Fe^{II}-NO during the course of the steady-state experiment.

The formation of Fe^{II}-NO can be observed indirectly by cyclic voltammetry. Limiting the potential window to a range from +0.20 to −0.40 V results in loss of the Fe^{III}/Fe^{II} redox couple after successive scans, Figure 3. Plotting the loss of the Fe^{III}/Fe^{II} couple with time gives a rate of dehydration of 9.0×10^{-3} s^{-1} for CYP119/DDAB in 34 mM nitrite. Under similar conditions, Mb/DDAB also exhibits a loss of the Fe^{III}/Fe^{II} redox couple under identical conditions at a rate of 9.2×10^{-3} s^{-1}, well within the experimental error of that for CYP119. This implies a similar mechanism is followed by both proteins. Indeed, we have recently reported that the solution reactivity of deoxy Mb with nitrite is zero order in Mb and first order in both nitrite and protons,[30] which again suggests that the initial step is dependent on the reaction of Fe^{II} with HONO, or its equivalent as NO^+.

Single Turnover Reduction of Fe^{II}-NO. For Mb/DDAB it was shown that, the $\mathbf{R_3}$ wave corresponds to the reduction of the ferrous NO adduct.[17] Using preformed NO−Mb/DDAB films, a reversible single-electron reduction was observed to a reduced nitroxyl species, $Fe^{II}\text{-}NO^-$ in eq 8, whose lifetime was pH-dependent. The intermediacy of nitric oxide can also be suggested in the electrochemical reduction of nitrite by CYP119 in surfactant film, but similar characterization of the single-electron reduction of the NO adduct is precluded because for CYP119 the ferrous NO adduct is unstable over the time needed to form a modified electrode.

$$Fe^{II}\text{-}NO + e^- \rightarrow Fe^{II}\text{-}NO^- \quad (8)$$

A simple method was derived to generate the NO adduct in situ via the reductive dehydration of nitrite. Holding the electrode potential at −0.40 V for 20 s prior to rapidly scanning to negative potentials resulted in a reversible redox couple at $E° = -0.85$ V vs Ag/AgCl, Figure 4, corresponding to the reduction of the ferrous nitrosyl to nitroxyl, eq 8. This behavior suggests that generation of the ferrous enzyme in the presence of nitrite results in formation of the nitrosyl enzyme and allows observation of the corresponding nitrosyl/nitroxyl redox couple. Under similar conditions and scan rates, Mb/DDAB also exhibits a redox couple corresponding to nitrosyl/nitroxyl reduction, at potential identical to that previously reported. As was seen for the preformed Mb−NO adduct,[17] the reversibility of this redox couple for CYP119 is strongly dependent on the scan rate, becoming more reversible as the scan rate is increased; a reversible signal, where $i_{pa}/i_{pc} = 1$, is only observed at scan rates > 1 V/s. At slower scan rates, the reduction is irreversible and the Fe^{III}/Fe^{II} redox couple reappears, Figure 5.

The heterogeneous rate constant for the reduction of the ferrous CYP119 NO adduct was obtained by simulation of voltammograms of ferrous NO generated in nitrite solutions, yielding $K^0 = 7.3 \times 10^{-2}$ cm/s (Supporting Information S14). As observed for Mb/DDAB, the reduced $Fe^{II}\text{-}NO^-$ in CYP119/DDAB film undergoes a pH dependent following reaction. Digital simulation of a single turnover reduction at pH 7 yields a rate of 45 s^{-1} for the irreversible loss of the Fe-coordinated NO; the comparable rate for Mb/DDAB is 22 s^{-1}.[17] It is our current supposition that this following reaction is the formation of the nitrosyl hydride adduct, Fe^{II}-HNO in eq 9, which we have shown to be unusually stable in aqueous solutions from pH 7 to 10.[16,30,31]

$$Fe^{II}\text{-}NO^- + H^+ \rightarrow Fe^{II}\text{-}HNO \quad (9)$$

Catalytic NO Reductions. To investigate the NoR activity of CYP119/DDAB, electrochemical studies were also performed under an atmosphere of nitric oxide, resulting the voltammetric response seen in Figure 11. As seen with Mb/DDAB, the redox couple associated with the Fe^{III}/Fe^{II} redox couple disappears upon addition of nitric oxide, and a catalytic wave develops at −0.82 V, close to the catalytic wave $\mathbf{R_3}$ in Figure 1, and approximately the same potential as the single electron reduction of the ferrous NO adduct, eq 8. Mass spectral analysis of the products of electrocatalytic reduction of ^{15}NO gives strong signals corresponding to $^{15}N_2O$ (46 *m*/*z*). The observed catalysis is substrate-limited, as indicated by the lack of steady-state current in Figure 11; at lower scan rates the current drop is lessened (Supporting Information S14). Increasing the scan rate results in the catalytic peak decreasing and the Fe^{III}/Fe^{II} redox couple reappearing (Supporting Information S15), but no reversibility was observed at the catalytic wave, i.e., no anodic current similar to that seen in Figure 4, even at scan rates as high as 20 V/s.

The irreversibility of the nitric oxide reduction couple is due to reaction of the ferrous-bound nitroxyl with nitric oxide from bulk solution. This models a key step in the enzymatic activity of cytochrome P450nor, as the last step in the catalytic cycle shown in Scheme 1. Digital simulations of catalytic voltammograms of the catalytic reduction of NO on a CYP119/DDAB

(30) Sulc, F.; Immoos, C.; Pervitsky, D.; Farmer, P. J. *J. Am. Chem. Soc.* **2004**, *126*, 1096.
(31) Sulc, F.; Fleischer, E.; Farmer, P. J.; Ma, D.; La Mar, G. *J. Biol. Inorg. Chem.* **2003**, *8*, 348.

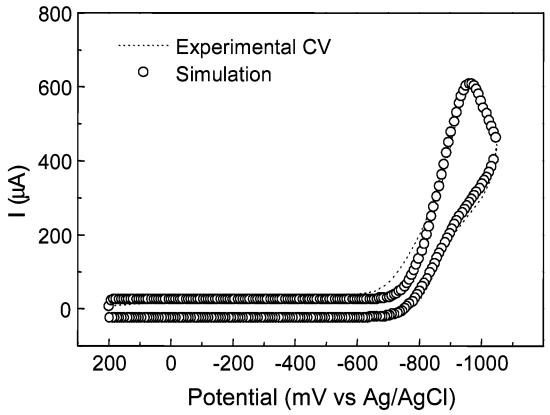

Figure 13. Experimental (dotted) and simulated (solid) cyclic voltammograms for CYP119/DDAB film electrode in saturated NO solutions. Conditions: 50 mM sodium phosphate; pH 7.0; 10 mM NaCl; scan rate = 3 V/s.

film were performed to obtain rate constants for the catalytic coupling step, Figure 13. Because of the similarity in catalytic voltammograms of NO reduction by Mb/DDAB,[17] the same mechanistic steps were used in the simulation, which encompass in sequence eqs 1, 10, 8, and 11.

$$Fe^{II} + NO \rightarrow Fe^{II}\text{-}NO \quad (10)$$

$$Fe^{II}\text{-}NO^{-} + NO + H^{+} \rightarrow Fe^{III} + N_2O + HO^{-} \quad (11)$$

The K_f of ferrous NO binding to CYP119, eq 10, is 1.1×10^7 M^{-1} s^{-1},[32] 2 orders of magnitude smaller than that of Mb, which is generally typical of P450 enzymes including P450nor.[33] Using these values, the digital simulation of a voltammogram of NO reduction in a saturated NO solution at pH 7 was obtained, Figure 13. K_{cat} value of the catalytic reaction of NO with Fe^{II}-NO^{-}, eq 11, was determined as 3×10^6 M^{-1} s^{-1}, significantly slower than that of Mb, at 1×10^8 M^{-1} s^{-1}. Thus, the thiolate ligation of CYP119 does not increase its effectiveness in N−N coupling reaction central to the P450nor reactivity.

Ammonia Incorporation during N_2O Formation. Certain denitrifying bacteria such as *P. stutzeri* and denitrifying fungi such as *Fusarium oxysporum*, can use a secondary nitrogen atom source such as azide, ammonium ion, and hydroxylamine to form N_2O under denitrifying conditions, a process termed "co-denitrification".[34] These secondary nitrogen sources are incapable by themselves of inducing N_2O production, but their incorporation into the gas during nitrite turnover is demonstrated by ^{15}N-labeling studies.[35] Our results show that both Mb and CYP119 can incorporate ammonia into the nitrous oxide produced during the catalytic reduction of nitrite.

In the quantification of ammonia production, Figure 7, we found that almost all the consumed nitrite is initially transformed into ammonia, but the efficiency significantly decreases as the electrolysis progresses. To test if solution-based ammonia is incorporated into N_2O, ^{15}N-labeled ammonia was added to natural abundance nitrite solution during bulk electrolysis by both Mb/DDAB and CYP119/DDAB, and indeed there was evidence by mass spectrometry of formation of $^{15}N^{14}NO$ (*m*/*z* 45) in both systems, Figure 9. For CYP119, the signal of $^{14}N^{14}NO$ is initially observed after 8 min, but a quite small signal of $^{15}N^{14}NO$ is only seen after 30 min and grew slowly during the electrolysis; the final ratio of two gases is 3.3:1 after 3 h. Under the same experimental conditions with Mb/DDAB as the electrocatalyst, the formation of $^{14}N^{14}NO$ is much higher initially, and the incorporation of the labeled ammonia, seen as the signal for mixed-labeled $^{15}N^{14}NO$, is greatly enhanced. After 3 h of electrolysis the mixed-label product becomes dominant, at a ratio of 1:1.3.

In both cases, a lag time is evident before label incorporation, which suggests that incorporation may be due to buildup of a transient, solution-based intermediate. The increased incorporation during catalysis by Mb/DDAB perhaps reflects the multitude of side products as seen in the product analysis. We had previously suggested that free NO^{-}, or HNO, was an initial byproduct of nitrite reduction by Mb/DDAB;[17] recent work has shown that HNO is electrophilic, for instance in its reaction with thiols that ultimately generates hydroxylamine and disulfide, eqs 12 and 13.[36] In this regard, a similar reactivity between HNO and labeled ammonia may lead to the mixed-labeled N_2O product. With this in mind, two possible HNO intermediates, trioxodinitrate and hyponitrite, were tested for incorporation labeled ammonia into the gaseous N_2O product. By this logic Angeli's salt decomposition, which generates HNO as in eq 14, would incorporate the labeled ammonia into the N_2O product; hyponitrite, which is the product of NO^{-} coupling and a direct precursor to N_2O, eqs 15 and 16, would not. As seen in the mass spectral chromatograms in Figure 10, the decomposition of hyponitrite upon addition of $^{15}NH_4^{+}$ indeed does generate the mixed-label $^{14,15}N_2O$ but, contrary to our expectations, that of Angeli's salt does not (Supporting Information S10). For both HNO precursors, addition of $^{15}NH_2OH$ led to generation of mixed-label $^{14,15}N_2O$. Thus attempts to identify the role of denitrification intermediates suggest that the hyponitrite anion $N_2O_2^{2-}$ may be involved in this co-denitrification, resulting in the formation of N_2O from ammonia.

$$HNO + RSH \rightarrow RS{-}NHOH \quad (12)$$

$$RS{-}NHOH + RSH \rightarrow NH2OH + RS{-}SR \quad (13)$$

$$Na_2N_2O_3 + H^{+} \rightarrow NO_2^{-} + HNO \quad (14)$$

$$2HNO \rightarrow H_2N_2O_2 \quad (15)$$

$$H_2N_2O_2 \rightarrow N_2O + H_2O \quad (16)$$

Catalytic Reduction of N_2O. As previously demonstrated for Mb/DDAB,[18] the Fe^{I} state of CYP119 is capable of catalytically reducing N_2O to N_2, Figure 12, formally a two-electron reduction. Evidence for such reactivity is that the addition of N_2O causes a significant increase in current at the Fe^{II}/Fe^{I} couple, along with a loss of reversibility, and that the irreversible current increases with increased N_2O concentrations. The Fe^{III}/Fe^{II} couple is not affected by the addition of substrate

(32) Scheele, J. S.; Bruner, E.; Kharitonov, V. G.; Martasek, P.; Roman, L. J.; Masters, B. S. S.; Sharma, V. S.; Magde, D. *J. Biol. Chem.* **1999**, *274*, 13105.
(33) Shiro, Y.; Fujii, M.; Iizuka, T.; Adachi, S.; Tsukamoto, K.; Nakahara, K.; Shoun, H. *J. Biol. Chem.* **1995**, *270*, 1617.
(34) (a) Tanimoto, T.; Hatano, K.; Kim, D.; Uchiyama, H.; Shoun, H. *FEMS Microbiol. Lett.* **1992**, *93*, 177. (b) Kumon, Y.; Sasaki, Y.; Kato, I.; Takaya, N.; Shoun, H.; Beppu, T. *J. Bacteriol.* **2002**, *184*, 2963.
(35) Laughlin, R. J.; Stevens, R. J. *Soil Sci. Soc. Am.* **2002**, *66*, 1540.
(36) (a) DeMaster, E. G.; Redfern, B.; Nagasawa, H. T. *Biochem. Pharmacol.* **1998**, *55*, 2007. (b) Demaster, E. G.; Redfern, B.; Quast, B. J.; Dahlseid, T.; Nagasawa, H. T. *Alcohol* **1997**, *14*, 181.

N_2O, indicating that N_2O does not bind to either oxidation state in CYP119/DDAB; as with nitrite dehydration, this reactivity is of the EC mechanism, electron transfer to produce the Fe^I state, followed by reaction with nitrous oxide, generating dinitrogen, eq 17. Here the catalytic efficiency of CYP119, at 107 turnovers/s under saturated solution, far exceeds that of Mb at 29 turnovers/s.

$$Fe^I + N_2O + H^+ \rightarrow Fe^{III} + N_2 + HO^- \qquad (17)$$

Conclusions

Cyclic voltammograms of electrocatalytic nitrite reduction by CYP119/DDAB are very similar to those previously reported for the analogous catalysis by Mb/DDAB: two catalytic waves at similar potentials are observed, the first corresponding to the reduction of nitric oxide, the second to the production of ammonia. The catalytic waves are highly pH-sensitive, and variation of nitrite concentrations demonstrates saturation kinetics. But analysis of the products shows that CYP119 is a much more selective catalyst, giving almost exclusively ammonia during the initial half-hour of reductive electrolysis. More careful investigations of specific steps in the catalytic cycle show comparable rates of nitrite dehydration, and almost identical potentials and lifetimes for ferrous nitroxyl intermediate (Fe^{II}-NO^-) in CYP119 and Mb. The catalytic efficiency of NO reduction is much reduced for CYP119 as compared to Mb; modeling suggests that the lower efficiency results from both a lower affinity of the protein for NO, as well as a decreased rate of N−N coupling. Isotopic studies show that the heme-protein modified electrodes perform biomimetic co-denitrification, and here again Mb/DDAB is much more active. Solution-based tests suggest that the hyponitrite anion $N_2O_2^{2-}$, rather than its immediate precursor, HNO, may be responsible for co-denitrification, resulting in the formation of mixed-label N_2O. Conversely, CYP119 is shown to be more efficient at the two-electron reduction of N_2O to N_2.

Our results suggest that thiolate ligation does not enhance or significantly alter the catalytic reactivity needed for P450nor activity. But the dramatic difference in product distribution suggests a major role of the protein itself: the rigidity and stability of the thermophilic CYP119 may be the controlling factor inhibiting side reactions, as demonstrated by the high yields of ammonia and low gaseous product formation.

Acknowledgment. We are deeply indebted to Thomas Poulos at University of California, Irvine, and Paul Ortiz de Montellano at University of California, San Francisco, for the several samples of CYP119 used in this work. This research was supported by the National Science Foundation (P.J.F.; Grant CHE-0100774). J.C. acknowledges funding by the Committee on Research, University of California, Irvine. C.E.I. and E.B. acknowledge graduate fellowships from the UC Toxic Substances Research and Teaching Program.

Supporting Information Available: Electronic absorbance spectra of CYP119/DDAB, plots of anodic current versus scan rate, and concentration dependence of nitrite reduction by CYP119/DDAB, a Lineweaver−Burke plot for electrocatalytic reduction of nitrite by CYP119/DDAB, a schematic describing the GC/MS setup, examples of mass spectral analysis and time-based GC-MS plots of ^{15}N-labeled gases, examples of chromatograms of headgas over HNO precursor solutions, and digital simulation of reversible reduction of Fe^{II}-NO species in CYP119. This material is available free of charge via the Internet at http://pubs.acs.org.

JA038925C